



## Original Article

Quantitative differences in the Y grain boundary excess at boundaries delimiting large and small grains in Y doped Al<sub>2</sub>O<sub>3</sub>Hadas Sternlicht<sup>a</sup>, Stephanie A. Bojarski<sup>b</sup>, Gregory S. Rohrer<sup>b</sup>, Wayne D. Kaplan<sup>a,\*</sup><sup>a</sup> Department of Materials Science and Engineering, Technion – Israel Institute of Technology, Haifa 32000, Israel<sup>b</sup> Department of Materials Science and Engineering, Carnegie Mellon University, Pittsburgh, PA 15213, USA

## ARTICLE INFO

## Keywords:

Grain boundary excess  
Complexion  
Alumina  
Abnormal grain growth

## ABSTRACT

The chemical excess at high angle grain boundaries in yttrium doped alumina was characterized using transmission electron microscopy and energy dispersive spectroscopy. The sample had a bimodal microstructure and one explanation for the fast growth of some grains was that they were surrounded by boundaries with a different yttrium grain boundary excess than the smaller grains. The amount of yttrium at boundaries between grains of similar and different sizes was quantified. Boundaries between smaller grains and between small grains bonded to sapphire had a mean Y excess of 1.3 atoms/nm<sup>2</sup>. The grain boundary excess of Y for boundaries delimiting large grains had either a lower Y content of 0.5 atoms/nm<sup>2</sup> and 0.9 atoms/nm<sup>2</sup>, or a higher Y content of 1.6 atoms/nm<sup>2</sup>, consistent with the idea that these boundaries had a different composition and thus different complexions.

## 1. Introduction

Doping polycrystalline  $\alpha$ -Al<sub>2</sub>O<sub>3</sub> (alumina) with Y has been shown to enhance bulk creep-resistance and to control grain growth. However, these results seem to be dependent on the processing conditions used to sinter the Y-doped alumina, leading to inconsistent conclusions in the literature [1–7]. Some investigations imply that the equilibrium grain boundary structure and chemistry (so called complexions [8]) in Y-doped alumina change when thermodynamic parameters (such as temperature and chemical composition) are changed, leading to a grain boundary state facilitating the increase of grain boundary mobility of certain grain boundaries [1,9–11].

Yttrium cations are nearly insoluble in the alumina lattice, with a bulk lattice solubility reported to be <10 ppm [12] or ~80 ppm [13]. At dopant levels below the solubility limit, Y adsorption to grain boundaries, which is driven by the reduction of grain boundary energy, will result in an Y excess, possibly changing the grain boundary properties. Above the solubility limit, the saturated grain boundary excess together with precipitates of the secondary phase may also change the grain boundary properties. It is believed that this excess, whether an equilibrium or transitory state, causes the enhanced creep resistance in the previously noted studies.

The concept of grain boundary complexions helps to explain the inconsistent results in the Y-doped alumina literature. In previously studied alumina, it has been shown that grain boundary mobility can

increase with increasing grain boundary excess for some dopants [14–16]. However, the addition of other dopants was found to decrease the grain boundary mobility [17]. The grain boundary atomistic structure depends on the grain boundary character (misorientation and grain boundary plane), as well as temperature and composition. As such, every specific grain boundary in a polycrystalline material has an equilibrium grain boundary state (complexion) at a defined temperature and pressure. Each grain boundary will then have a specific activation energy required for transitions between equilibrium states (complexions). This is further complicated by the fact that the decrease in grain boundary area with increasing grain size during grain growth, if local equilibrium is maintained, drives dopant ions either into the lattice (at dopant concentrations below the solubility limit), or into second phase precipitates (at dopant concentrations above the solubility limit). Shrinking grain boundary area may also lead to a super-saturated metastable state if the barrier for forming second phase precipitates is large. Given the extremely low solubility limit of Y in alumina, it is likely that secondary phase precipitates play a role, together with grain boundary complexions, on defining creep rates and grain boundary mobility.

Microstructural characterization of Y-doped alumina has shown microstructures ranging from a fine-grained uni-modal grain size distribution to a nearly bi-modal grain size distribution, where large and small grains coexist in the same microstructure [1,9,10]. It has also been shown that abnormally fast grain growth in Y-doped alumina also

\* Corresponding author.

E-mail address: [kaplan@technion.ac.il](mailto:kaplan@technion.ac.il) (W.D. Kaplan).

initiates a shift in the preferred grain boundary plane from  $(110\bar{2})$  to  $(11\bar{2}0)$  [1]. This implied that grain boundaries of specific character were lower in energy, and thus encompassed a larger surface area in the (near) equilibrium microstructure, or that specific growth directions have a higher mobility thus leading to a kinetically defined microstructure. Once the Y-doped alumina microstructure reached a unimodal grain size distribution of (apparently) impinged abnormal grains, the  $(11\bar{2}0)$  grain boundary plane was three times more likely to occur in the microstructure while the  $(0001)$  plane was least likely to occur [1]. It has since been found that grain boundaries with one plane near  $(11\bar{2}0)$  have a lower energy than grain boundaries with one plane near  $(0001)$  [9].

The grain boundary character and increased mobility of Y-doped alumina grain boundaries are indicative of the role of complexions in microstructural evolution. This is supported by the conclusions drawn by Voytovych et al. indicating that an increased growth rate above 1550 °C resulted from a transition between grain boundary diffusion and lattice diffusion driven densification [18]. However, the bimodal nature of the microstructural development does not lend convincing evidence to that conclusion. From studies on Y-doped alumina containing a secondary phase (i.e. above the solubility limit), Wang et al. concluded that there is a level of equilibrium Y solute adsorption to grain boundaries which is equivalent to  $\frac{1}{4}$  an equivalent monolayer ( $3.2 \pm 0.8$  Y atoms/nm<sup>2</sup>) [19]. This amount of segregated Y at grain boundaries was correlated to the coexistence of segregated Y at grain boundaries and precipitation of YAG particles. Before reaching this equilibrium value, the boundaries become super-saturated, and at this point  $\frac{1}{2}$  an equivalent monolayer of Y ( $5.1 \pm 0.2$  Y atoms/nm<sup>2</sup>) is adsorbed to these boundaries [19].

These results paired with the changes in mesoscale properties observed in this system indicate that grain boundary complexion transitions may affect the mechanism of grain growth leading to abnormal grain growth, or reduce specific grain boundary energies leading to anisotropic morphologies. Additional dopant ions (or impurities) may also be important, and abnormal grain growth has been correlated with combined Y – Si segregation [10,20]. The current work addresses accelerated grain growth observed in Y-doped alumina in terms of grain boundary complexion transitions and interfacial energies. Changes in the mobility of these boundaries may depend on the grain boundary properties such as energy and misorientation, as well as changes in the Y composition of a given boundary. As such, this work aims to accurately quantify the Y composition differences between large and small grains, and high and low energy interfaces, in Y-doped Al<sub>2</sub>O<sub>3</sub> with a bimodal grain size.

## 2. Experimental methods

### 2.1. Y doped Al<sub>2</sub>O<sub>3</sub> samples

Alumina powder doped with 500 ppm of Y was prepared using standard powder processing techniques as described in [9]. Sapphire crystals with both  $(0001)$  (C-plane) and  $(11\bar{2}0)$  (A-plane) orientations (MTI Corp, Richmond, CA) were cleaned to remove any metallic or organic residue. The doped powders were placed into a graphite die between the C-plane and A-plane oriented sapphire crystals. Sacrificial Y-doped alumina powder was placed between the graphite die and the samples to minimize contamination.

The die was uniaxially pressed to form a green compact, then spark plasma sintered (SPS; Thermal Technologies, LLC, Santa Clara, CA) using the following thermal treatment: a ramp of 100 °C/min to 800 °C at a pressure of 10 MPa for an initial calcination dwell of 45 min, followed by an additional 100 °C/min ramp to 1300 °C for sintering at 50 MPa for 30 min. After sintering, the sample was sectioned, cleaned, and annealed in an open-air box furnace (Lindberg/Blue M 1700 °C box furnace, Riverside, MI) for 1500 °C for 4 h. The sample was then manually removed while still at 1500 °C and immediately quenched in

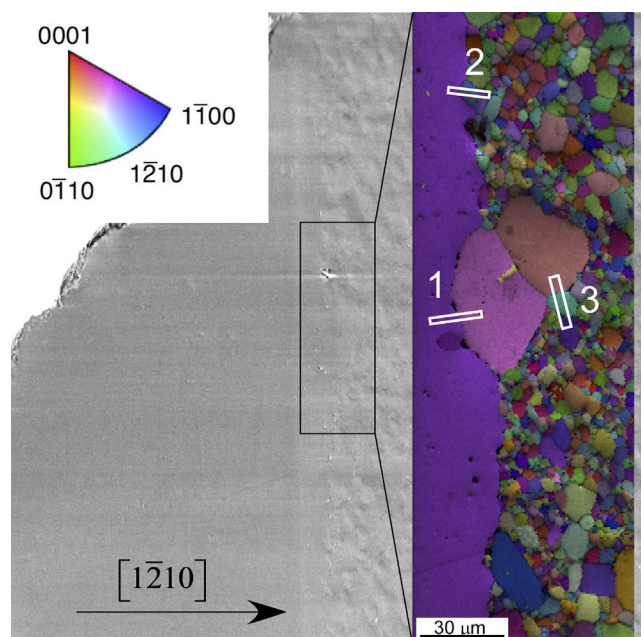


Fig. 1. An EBSD map of a diffusion bonded sample, showing the A plane single crystal and the Y doped polycrystalline alumina. The orientation map is colored with respect to the image normal. The areas next to the A plane from which TEM samples were prepared are marked. Area 1 was used for (A)-AG sample, area 2 was used for NG- NG near (A) and (A)-NG samples, and area 3 was used for AG- NG near (A) sample. NG stands for normal grain, AG for abnormal grain, and (A) for the A plane single crystal of the sample.

liquid nitrogen to preserve the high temperature state of the grain boundaries. The samples were then polished to a colloidal silica finish.

Electron backscatter diffraction (EBSD) orientation maps were collected along both embedded single crystal interfaces. This was done to both orient the sample and to map where abnormal grain growth occurred. Fig. 1 shows an example EBSD map, and diagram explaining from where transmission electron microscopy (TEM) samples were taken along the  $(11\bar{2}0)$  single crystal interface.

### 2.2. Characterization methods

The samples were characterized using aberration corrected TEM (FEI Titan 80–300 kV S/TEM). TEM samples were prepared using the lift-out technique using a dual-beam focused ion beam (FIB; FEI Strata 400 s and FEI Quanta 3D), focusing on boundaries between the single crystal and a grain in the polycrystalline material, and boundaries in the polycrystalline section which were close to the single crystal [21].

For each TEM sample, Kikuchi electron diffraction was used to orient one of the grain boundary delimiting grains into a low-index zone axis, where the grain boundary plane was close to parallel to the incident electron beam (edge-on condition). Then sets of energy dispersive spectroscopy (EDS) measurements were acquired from three regions of equivalent area; one inside each of the grains and one region including the grain boundary. The thickness of each region that was characterized using EDS was determined using the plasmon signal from electron energy loss spectroscopy (EELS).

#### 2.2.1. Spatial difference technique

The spatial difference technique is based on two EDS (or EELS) measurements in the bulk, from a defined volume of material adjacent to a selected grain boundary in both of the grains that form the boundary, and an additional measurement from an identical volume of material containing the grain boundary. The solute signal acquired from the bulk is removed from that of the boundary, and the residual signal represents the amount of solute associated with an excess (which can be negative) at the boundary. The amount of excess (atoms/nm<sup>2</sup>)

can be determined from [22–26]:

$$\Gamma = \frac{V}{S} \frac{A_B}{A_A} \rho k_{AB} \frac{I_A}{I_B} \quad (1)$$

where  $V/S$  is the ratio between the interaction volume to the area of the grain boundary inside the interaction volume,  $\rho$  is the matrix density in ( $\text{kg}/\text{m}^3$ ),  $A_A$ ,  $A_B$ ,  $I_A$  and  $I_B$  are the atomic mass in ( $\text{kg}/\text{mol}$ ) and measured intensities for the matrix and excess species (after subtracting the same signals acquired from the adjacent bulk grains), respectively, assuming  $c_A + c_B = 1$ . The detection limit of this method is

$$\Gamma_{\min} = \frac{V}{S} \frac{A_B}{A_A} \rho k_{AB} 3 \frac{\sqrt{2I_A^b}}{I_B} \quad (2)$$

where  $I_A^b$  is the background intensity under the peak of interest [22–26]. The k-factor value has to be measured from a standard sample, following the Cliff Lorimer equation [24]:

$$\frac{C_A}{C_B} = k_{AB}^* \frac{I_A}{I_B} \quad (3)$$

The measured k-factor has to be corrected for absorption of the X-ray photons by the sample itself. The corrected k-factor,  $k_{AB}^*$ , is thus:

$$k_{AB}^* = ACF^* k_{AB} \quad (4)$$

where the absorption correction factor (ACF) is [24]:

$$ACF = \frac{\int_{Spec}^A \frac{\mu}{\rho} 1 - e^{-\int_{Spec}^B \frac{\mu}{\rho} \rho t'} dt'}{\int_{Spec}^B \frac{\mu}{\rho} 1 - e^{-\int_{Spec}^A \frac{\mu}{\rho} \rho t'} dt'} \quad (5)$$

where  $\int_{Spec}^A \frac{\mu}{\rho}$  is the sum of the mass absorption coefficients of X rays from element A multiplied by the weight fraction of that element in the specimen,  $\rho$  is the density, and  $t'$  is the x ray absorption length. For a flat sample  $t' = t/\sin\alpha$ , where  $t$  is the thickness of the sample, and  $\alpha$  is the angle between an axis perpendicular to the electron beam direction and a X ray reaching the detector [24].

The thickness can be determined from EELS using:

$$\frac{t}{\lambda} = \ln\left(\frac{I_T}{I_{ZLP}}\right) \quad (6)$$

where  $t$  is the thickness,  $\lambda$  is the plasmon mean free path,  $I_T$  is the total integrated area under the EELS spectrum, and  $I_{ZLP}$  is the area under the zero loss peak. Thus, by multiplying an experimental EELS thickness map of  $\ln(I_T/I_{ZLP})$  by the plasmon mean free path for the selected material, the thickness can be accurately determined. The plasmon mean free path can be experimentally measured using the technique developed by Meltzman et al. [27].

### 3. Results

The intensities of the K lines for Y and Al were determined from EDS measurements using the spatial different technique. To quantify the amount of Y at the studied grain boundaries according to Eq. (1), an experimentally determined k-factor was measured from a standard sample and corrected for absorption.

#### 3.1. k-Factor

To measure k-factors for Y-doped  $\text{Al}_2\text{O}_3$  samples, YAG ( $\text{Y}_3\text{Al}_5\text{O}_{12}$ ) was used as a standard. The mean free path of plasmons in YAG was measured from a thickness map of a YAG sample in the shape of a needle using the technique developed by Meltzman et al. [27]. Following this technique, the thickness divided by the mean free path of

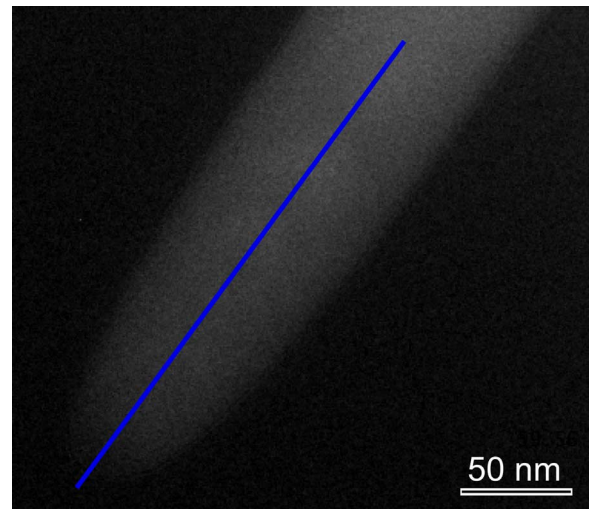


Fig. 2. A thickness map ( $t/\lambda$ ) of the standard YAG needle shaped sample. A line along which EDS intensities and thickness were measured, is marked along the center of the sample.

plasmons in YAG ( $t/\lambda$ ) was measured along the length of a YAG needle-shaped sample (shown in Fig. 2), as a function of the width of the sample (for conical needles, the width is equivalent to the thickness). From the slope of the acquired graph (acquired using regression of the measurements plotted in Fig. 3), the mean free path of plasmons in YAG was found to be  $\lambda_{\text{YAG}} = 153 \pm 3 \text{ nm}$ .

From an EDS line-scan along the center of the YAG needle, the K line intensities of Al and Y were measured as a function of thickness. The thickness at each point was determined from a thickness map ( $t/\lambda$ ) multiplied by the experimentally determined plasmon mean free path in YAG. The measured intensities were corrected using the absorption correction factor (Eq. (5)), where the mass absorption coefficients of the single elements were taken from [28], and the thickness was experimentally measured. The parameters used for this calculation are listed in Table 1. Since the needle is conical in shape,  $t' \approx t$ .

The corrected intensities (for example  $\frac{I_Y}{1 - e^{-\int_{Spec}^Y \frac{\mu}{\rho} \rho_{YAG} t}} \frac{1}{\int_{Spec}^Y \frac{\mu}{\rho} \rho_{YAG} t}$ )

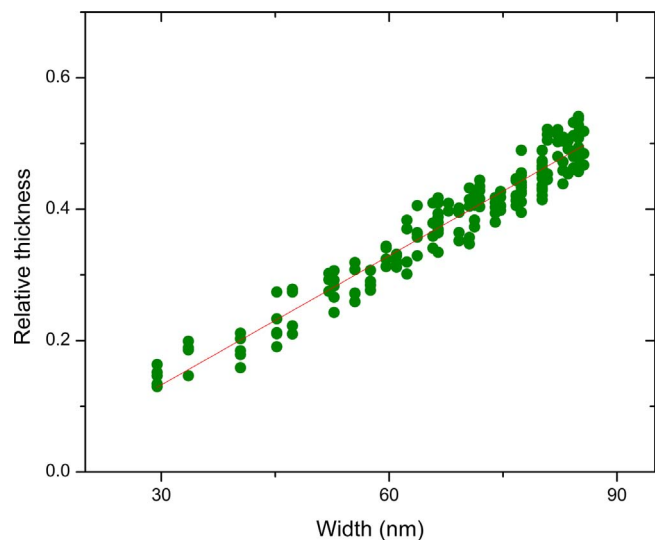
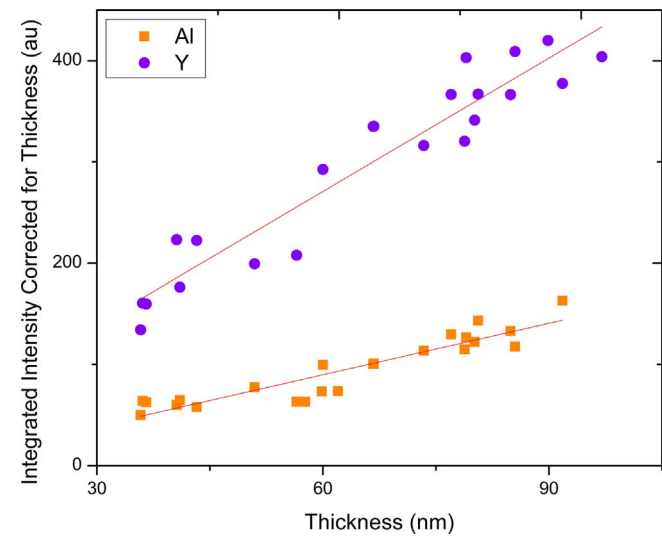


Fig. 3. A  $t/\lambda$  line-scan, acquired along the blue line in Fig. 2 running along the length of the needle. The linear fit is plotted in red ( $R^2 = 0.94$ ).

**Table 1**  
Mass absorption coefficients used for the quantitative analysis of EDS data [28].

$$\begin{aligned} \mu/\rho_{Al(Al\ K\alpha)} &= 422\text{cm}^2/\text{gr} \\ \mu/\rho_{Al(Y\ K\alpha)} &= 8.98\text{cm}^2/\text{gr} \\ \mu/\rho_{Y(Al\ K\alpha)} &= 1600\text{cm}^2/\text{gr} \\ \mu/\rho_{Y(Y\ K\alpha)} &= 23.7\text{cm}^2/\text{gr} \\ \mu/\rho_{O(Al\ K\alpha)} &= 1570\text{cm}^2/\text{gr} \\ \mu/\rho_{O(Y\ K\alpha)} &= 1.85\text{cm}^2/\text{gr} \\ \mu/\rho_{Spec}^Y &= 0.323*1.85 + 0.227*8.98 + 0.449*23.7 = 13.288\text{cm}^2/\text{gr} \\ \mu/\rho_{Spec}^{Al} &= 0.323*1570 + 0.227*422 + 0.449*1600 = 1322.581\text{cm}^2/\text{gr} \\ \rho_{YAG} &= 4.56\text{gr}/\text{cm}^3 \\ \theta &= 20.1^\circ \end{aligned}$$


**Fig. 4.** The integrated intensity corrected for thickness of the K lines of Y and Al from an EDS line-scan along the center of the YAG needle, which is thus as a function of thickness. ( $R^2$  is 0.91 for Y and 0.86 for Al).

as a function of thickness are presented in Fig. 4. Following the Cliff Lorimer equation (Eq. (3)), we can divide the corrected intensities measured from the standard sample in order to extract the k-factor which is not corrected for absorption,  $k_{Y-Al}$ :

$$\frac{C_Y}{C_{Al}} = k_{Y-Al}^* \frac{I_Y}{I_{Al}} = \frac{I_Y}{\frac{1 - e^{-\mu/\rho_{Spec}^Y \rho_{YAG} t}}{\mu/\rho_{Spec}^Y \rho_{YAG} t}} \frac{1 - e^{-\mu/\rho_{Spec}^{Al} \rho_{YAG} t}}{\mu/\rho_{Spec}^{Al} \rho_{YAG} t}}{I_{Al}} k_{Y-Al} \quad (7)$$

By dividing the slopes of the curves presented in Fig. 4 using (7), we can determine the k-factor which is not corrected for thickness. The measured value was found to be  $k_{Y-Al} = 0.76 \pm 0.09$ .

### 3.2. Spatial difference technique measurements on Y doped $Al_2O_3$ grain boundary samples

#### 3.2.1. k-factor

Since Y was found only at grain boundaries (this will be shown in the next sections), the main absorber of the X-ray photons from the diffusion bonded sample was alumina. To determine the thickness of the areas that were characterized, EELS thickness maps ( $t/\lambda$ ) were multiplied by the measured mean free path of plasmons in alumina ( $\lambda_{Al_2O_3} = 143\text{nm}$ [27]).

The k-factor for each set of spatial difference measurements was

**Table 2**  
Mass absorption coefficients used for the quantitative analysis of EDS data [28].

$$\begin{aligned} \mu/\rho_{Spec}^Y &= 0.47*1.85 + 0.53*8.98 = 5.629\text{cm}^2/\text{gr} \\ \mu/\rho_{Spec}^{Al} &= 0.47*1570 + 0.53*422 = 961.56\text{cm}^2/\text{gr} \\ \rho_{Al_2O_3} &= 3.9\text{gr}/\text{cm}^3 \end{aligned}$$

determined using the  $k_{Y-Al}$  that was extracted above, and the absorption coefficients of the single elements found in [28] using Eq. (5). The take-off angle of the detector was  $20.1^\circ$ , thus  $\alpha = 20.1 \pm \alpha'$  where  $\alpha'$  is the tilt angle of the sample. In practice, because the actual thickness was measured for each measurement and the thickness of the FIB samples is not uniform, the tilt angle of the sample was neglected. This introduces a small error, which is in the order of  $\sim 0.01$  atoms/nm<sup>2</sup>. By keeping the tilt angle constant for the measurements from a certain boundary the resulting error remained constant for the whole set of measurements. The parameters used for this calculation are listed in Table 2.

#### 3.2.2. Deviation from edge-on conditions

When measuring the amount of dopants at grain boundaries, the boundary is required to be parallel to the incident electron beam (edge-on imaging condition). The error in the measured excess at a grain boundary due to inclination of the boundary plane from edge-on conditions was dealt with by Williams et al. [26] by formulating the measured intensity from the boundary. In their calculation both the electron probe shape distribution and the actual compositional distribution were taken into account. When using the spatial difference method for this task, the electron probe shape distribution is redundant [15,29]. Thus, the excess in an inclined boundary can be estimated using a geometric approach, by evaluating V/S in Eq. (1). When the boundary is edge-on:

$$\left. \begin{aligned} V &= abh \\ S &= bh \end{aligned} \right\} V/S = a \quad (8)$$

where  $a$  and  $b$  are the width of the scan perpendicular and parallel to the boundary, respectively, and  $h$  is the thickness of the sample. When the boundary is inclined to the incident electron beam:

$$\left. \begin{aligned} V &= abh \\ S &= hb^1/\cos \omega \end{aligned} \right\} V/S = a \cos \omega \quad (9)$$

where  $\omega$  is the inclination angle from edge-on conditions. Thus

$$\Gamma_{\text{tilted}} = \Gamma_{\text{edge on}} \cos \omega \quad (10)$$

Some examples of errors resulting from inclination from edge-on conditions are presented in Fig. 5, indicating that when determining the excess of a dopant at a grain boundary, small deviations from the edge-on condition will not cause a significant change in the measured value.

#### 3.2.3. Y amounts at different boundaries

For each grain boundary, several EDS measurements using the spatial difference technique were acquired along the boundary. The Y content of each grain boundary was determined using Eq. (1), which was modified for the measured system:

$$\Gamma = \frac{V}{S} \frac{2A_{Al}}{A_Y} \rho k_{Y-Al}^* \frac{I_Y}{I_{Al}} \quad (11)$$

The k-factor was determined using  $k_{Y-Al}$  that was described above, and corrected for absorption using the ACF where the local thickness of the measured area was extracted from a thickness map multiplied by  $\lambda_{Al_2O_3}$ . For each boundary, the average Y content and standard deviation

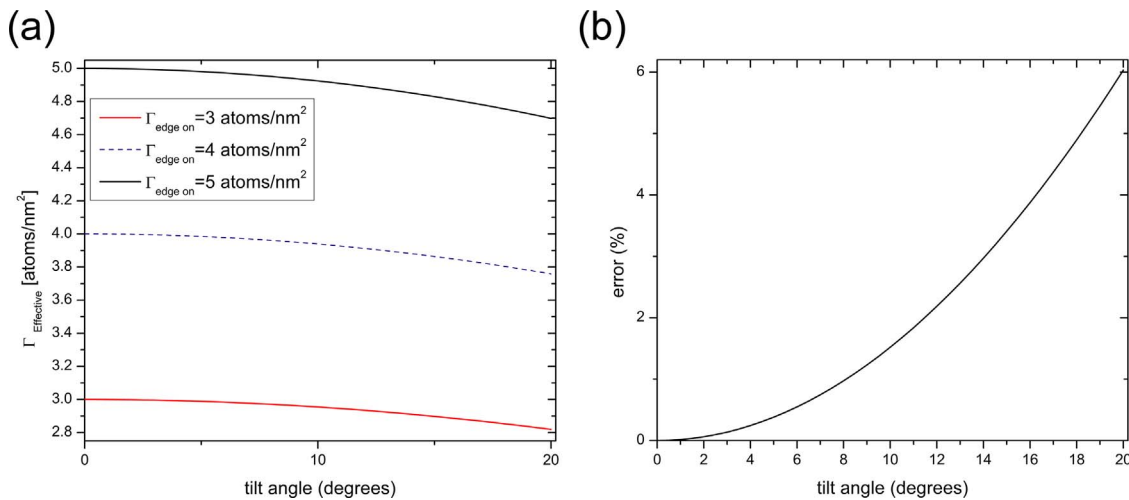


Fig. 5. (a) The value of excess measured using the spatial difference technique as a function of deviation from the edge-on condition, and (b) the relative error for all excess values presented in (a).

were determined.

For thick samples (which were used to increase the EDS counts), in which the mean free path of plasmons does not depend linearly on the thickness, the mean free path of plasmons was extracted from a calibration curve acquired from a thicker region of an  $\text{Al}_2\text{O}_3$  needle. Fig. 6 presents the excess of Y measured at the studied boundaries. The error bars represent the standard deviation of the average amount of Y measured at different areas along each of the boundaries.

### 3.2.4. Detection limit

To determine the detection limit of the measurements, the detection limit was determined for each set of spatial difference measurements:

$$\Gamma_{\min} = \frac{V}{S} \frac{2A_{\text{Al}}}{A_{\text{Y}}} \rho k_{\text{Y-Al}}^* 3 \frac{\sqrt{2I_{\text{Y}}^b}}{I_{\text{Al}}} \quad (12)$$

The mean EDS detection limit was 0.2 atoms/nm<sup>2</sup>, acquired as an average value from all of the excess measurements. Y was not detected inside the bulk grains with an average EDS bulk detection limit of ~0.03 wt.% (300 ppm) which was determined using:

$$C_{\min}^{\text{Y}} = \frac{3\sqrt{2I_{\text{Y}}^b} C^{\text{Al}} k_{\text{Y-Al}}^*}{I_{\text{Al}} \sqrt{m\tau}} \quad (13)$$

where  $m$  is the number of measurements,  $\tau$  is the acquisition time, and the Al bulk concentration is assumed to be  $C^{\text{Al}} \approx 1$  (since  $C^{\text{Y}} \ll 1$  and  $C^{\text{Y}} + C^{\text{Al}} = 1$ ).

## 4. Discussion

In a separate study of this specimen, YAG precipitates have been observed, so we can be certain that both the bulk and the grain boundaries are saturated with Y [30]. Measurement of relative grain boundary energies from grain boundary thermal grooves showed that the mean energy of a 500 ppm Y doped  $\text{Al}_2\text{O}_3$  was less at 1550 °C compared to measurements made at 1450 °C [30]. Both the decreasing mean grain boundary energy and the bimodal distribution suggest the coexistence of grain boundaries with multiple complexions [31]. In Fig. 6 it can be seen that boundaries between normal grains, and between normal grains and the sapphire crystal, contain a mean Y excess of 1.3 atoms/nm<sup>2</sup>. For these boundaries, the proximity to the C plane or A plane showed no clear influence on the Y excess. Boundaries with one abnormal grain had a range of grain boundary excess values that was above or below that of the boundaries between small grains. In these boundaries, the second grain creating the boundary in addition to the abnormal grain was either a normal grain or the single crystal. One very interesting finding is that in boundaries where one grain was an abnormal grain, the Y excess at the boundary with the (11 $\bar{2}$ 0) oriented crystal is larger than at the (0001) oriented crystal. A study of the relative energies of such boundaries found that the boundaries with the (11 $\bar{2}$ 0) crystal had a lower energy than the boundaries with the (0001) crystal [9]. In the most simple formulation of grain boundary segregation, a larger Y excess should be correlated with a lower energy.

The error bars in Fig. 6 indicate that within the eight studied boundaries, variations in the Y content can exist along each of the boundaries. Such a variation could occur due to changes in the structure and chemistry along a boundary. While we would expect the structure and chemistry of different facets to vary, the detection of

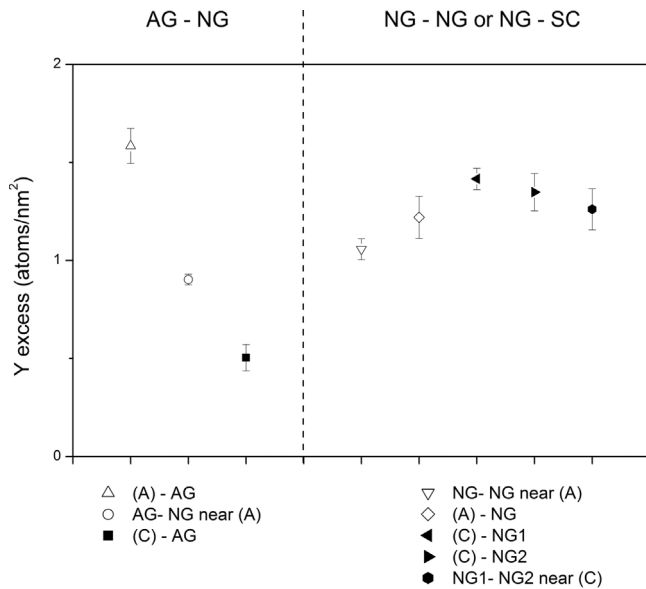


Fig. 6. Y excess measured at different grain boundaries. NG stands for normal grain, AG for abnormal grain, SC for single crystal (either A plane or C plane) and (A) and (C) for the A plane and C plane single crystals of the sample. Each data point is an average between several measurements along the same boundary; 3 in (A)-AG, 4 in AG-NG near (A), 6 in (C)-AG, 4 in NG-NG near (A), 4 in (A)-NG, 9 in (C)-NG1, 3 in (C)-NG2 and 5 in NG1-NG2 near (C). The results are separated according to the type of single crystal the boundary is close to (or act as one of the delimiting grains) and the size of the delimiting grains in the polycrystalline part of the sample. Filled and empty markers represent boundaries between or next to the C and A plane respectively. On the left boundaries between an abnormal grain and a normal grain are presented (marked as AG-NG). On the right boundaries between normal grains or a single crystal and a normal grain are presented (marked as NG-NG or NG-SC).

facets is straightforward and thus should not introduce a source of error. However, steps at the atomic length-scale certainly exist along grain boundary facets, but they are not always detectable by the various imaging techniques. As such, analysis of facet segments without steps may result in a chemical content different from facet segments with steps. In addition, different sections of facets with steps would result in different atomistic structures and chemical excess. As a result there would be a difference in the amount of sites to which Y atoms could be introduced and thus different amounts of Y atoms. In addition, kinetic factors may also contribute to variations in the Y excess along the boundary. Variations in dopant content along grain boundaries was also reported elsewhere [13,19,32].

Gruffel and Carry showed that upon an increase in grain size and with an increase in doping, the Y excess at grain boundaries first increased monotonically, and then saturated at a rather constant value when YAG precipitation occurred [14]. Wang et al. later proposed that supersaturation can occur before the plateau value is reached and precipitation of YAG occurred [19]. This was also measured by Gulgun et al. who divided the segregation behavior of Y in  $\text{Al}_2\text{O}_3$  grain boundaries into three regions; (1) dilute adsorption in which the Y excess increased with the total Y doping amount following hypothetical curves that assume Y adsorption only to grain boundaries (calculated for the measured grain size assuming that Y segregated equally to all grain boundaries and negligible dissolution of Y in the bulk), (2) a supersaturation region where the Y content reached a maximum value deviating from the calculated hypothetical perfect adsorption curve and Langmuir-McLean behavior, and (3) the Y content reached a plateau value and YAG precipitates form [15]. Based on previous observations of YAG in the samples in the present study, these samples are in the third region. While in the current work the excess of Y at grain boundaries was not measured as a function of Y solute concentration, or a strict measurement of grain size, variation in the Y amount is still expected, as discussed above.

The results presented here also indicate that the amount of Y excess at grain boundaries can vary while having a maximum value of 1.6 atoms/nm<sup>2</sup>. Larger amounts of Y atoms at grain boundaries were previously correlated to larger grain sizes [14,15]. In agreement with the literature, the largest amount of Y excess measured in this work was detected at a boundary between an abnormal grain and the crystal with the (11 $\bar{2}$ 0) orientation. The largest amount of Y excess in this specific boundary can be also correlated to the low energy of boundaries with the (11 $\bar{2}$ 0) single crystal which could result from the large amount of Y excess at the boundary [9]. We assume that the two smallest amounts of Y excess measured here (at a boundary between an abnormal grain and a normal grain and at a boundary between an abnormal grain and the (0001) single crystal) could result from three possible cases. The first is the formation of YAG precipitates after the boundary reached a maximum value of excess (grain boundary saturation), which will cause a depletion of Y atoms from the boundary and the bulk (in the vicinity of the boundary). A similar approach was also suggested by MacLean et al. [10]. A second possibility could be simple kinetic reasons, where either Y was slow to arrive to the grain boundary, or less Y accumulated at a moving grain boundary. A third possibility could be differences in the structure of the studied boundaries, where specific boundaries may have less sites to accommodate excess atoms. The lowest amount of Y excess at a boundary between an abnormal grain and the (0001) single crystal can also be attributed to the high relative energy of boundaries with the C plane [9].

It was suggested in the literature that boundaries with abnormal grains go through a complexion transition from a low mobility complexion to a high mobility more stable complexion. In a sandwich sample similar to the one used for the present study, such a transition was shown to occur more extensively at the high energy C plane interface rather than at the interface with A plane sapphire. While such boundaries can go through a complexion transition, it is possible that only some of the boundaries surrounding an abnormal grain have

transformed. The results presented here indicate that boundaries delimiting an abnormal grain have a different Y content, which suggests the presence of one or more complexions different from those at boundaries between normal grains, and between normal grains and a single crystal. The influence of the orientation of the single crystal on the complexion transition at boundaries which delimit an abnormal grain cannot be addressed using the results presented here, due to the limited amount of characterized boundaries [9,31].

The present observations are consistent in magnitude with previous measurements of Y grain boundary excess in Y doped  $\text{Al}_2\text{O}_3$ . The past observations reported values of 9, 6–7 atom/nm<sup>2</sup> [15], 1.5–6 atoms/nm<sup>2</sup> [33], and a maximum value of  $5.1 \pm 0.2$  atoms/nm<sup>2</sup> which dropped to a constant value of  $3.2 \pm 0.8$  atoms/nm<sup>2</sup> once the overall dopant concentration was increased [19]. In all of these reports, sample preparation was done using conventional sintering. While the sample studied in this work was prepared using SPS, the measured Y values are near to the reported values. In several studies, impurities/dopants other than Y were present (such as Si, Mg or Zr), which may have affected the measured Y content, and further explain the deviation from the values measured in this work [14,15,33,34]. The k-factor used in the literature varies; 1.36 was experimentally determined (for a specific thickness) compared to the theoretically calculated value of 2.109 (from EDS software) [15], 4.5 [33], 1.25 [19], and 1.36 extracted from extrapolation of k values calculated using the Cliff Lorimer Eq. (3) as a function of estimated local thickness in a standard [32]. While this value is unique for a certain experimental setting (and varies with EDS detector and instrument, experimental system, take off angle and sample thickness) the use of a constant value within a set of measurements (without corrections) as done in the literature further contributes to the deviations from the excess values measured here (after measuring the k-factor which is suitable for the specific measurements done in this manuscript).

## 5. Summary and conclusions

The Y excess content was measured at different general grain boundaries between grains of different sizes. To accurately measure the amount of Y excess, the mean free path of plasmons in YAG was measured to determine the local thickness, and the k-factor was measured as a function of thickness. For boundaries between normal grains, there were no significant differences for boundaries next to or including the C or A orientation of the single crystals. However, boundaries between an abnormal grain and a normal grain or a single crystal deviated in Y content from the boundaries between normal grains. Boundaries between an abnormal grain and the A plane single crystal, and an abnormal grain and the C plane single crystal showed the highest and lowest amounts of Y excess, respectively. This can be attributed to the lower relative energy of boundaries with the A plane compared to boundaries with the C plane resulting from the difference in the amount of Y excess.

## Acknowledgements

SAB and GSR acknowledge support from the ONR-MURI program (grant no. N00014-11-0678). The authors also acknowledge use of the Materials Characterization Facility at Carnegie Mellon University supported by grant MCF- 677785.

## References

- [1] S.A. Bojarski, M. Stuer, Z. Zhao, P. Bowen, G.S. Rohrer, Influence of Y and La additions on grain growth and the grain-boundary character distribution of alumina, *J. Am. Ceram. Soc.* 97 (2) (2014) 622–630.
- [2] H. Yoshida, Y. Ikuhara, T. Sakuma, High-temperature creep resistance in rare-earth-doped, fine-grained  $\text{Al}_2\text{O}_3$ , *J. Mater. Res.* 13 (9) (1999) 2597–2601.
- [3] J.P. Bujan, K. Matsunaga, J. Chen, N. Shibata, W.Y. Ching, T. Yamamoto, Y. Ikuhara, Grain boundary strengthening in alumina by rare earth impurities,

- Science 311 (5758) (2006) 212–215.
- [4] J. Cho, M.P. Harmer, H.M. Chan, J.M. Rickman, A.M. Thompson, Effect of yttrium and lanthanum on the tensile creep behavior of aluminum oxide, *J. Am. Ceram. Soc.* 80 (4) (1997) 1013–1017.
- [5] T. Sakuma, Y. Ikuhara, Y. Takigawa, P. Thavorniti, Importance of grain boundary chemistry on the high-temperature plastic flow in oxide ceramics, *Mater. Sci. Eng.: A* 234 (1997) 226–229.
- [6] J.D. French, J. Zhao, M.P. Harmer, H.M. Chan, G.A. Miller, Creep of duplex microstructures, *J. Am. Ceram. Soc.* 77 (11) (1994) 2857–2865.
- [7] J. Cho, C.M. Wang, H.M. Chan, J.M. Rickman, M.P. Harmer, Role of segregating dopants on the improved creep resistance of aluminum oxide, *Acta Mater.* 47 (15) (1999) 4197–4207.
- [8] W.D. Kaplan, D. Chatain, P. Wynblatt, W.C. Carter, A review of wetting versus adsorption, complexions, and related phenomena: the rosetta stone of wetting, *J. Mat. Sci.* 48 (2013) 5681–5717.
- [9] S.A. Bojarski, M.P. Harmer, G.S. Rohrer, Influence of grain boundary energy on the nucleation of complexion transitions, *Scr. Mater.* 88 (2014) 1–4.
- [10] I. MacLaren, R.M. Cannon, M.A. Gülgün, R. Voytovych, N. Popescu-Pogrión, C. Scheu, U. Täffner, M. Rühle, Abnormal grain growth in alumina: synergistic effects of yttria and silica, *J. Am. Ceram. Soc.* 86 (4) (2003) 650–659.
- [11] P.R. Cantwell, M. Tang, S.J. Dillon, J. Luo, G.S. Rohrer, M.P. Harmer, Grain boundary complexions, *Acta Mater.* (Supplement C) (2014) 1–48.
- [12] J.D. Cawley, J.W. Halloran, Dopant distribution in nominally yttrium-doped sapphire, *J. Am. Ceram. Soc.* 69 (8) (1986) C-195–C-196.
- [13] A.M. Thompson, K.K. Soni, H.M. Chan, M.P. Harmer, D.B. Williams, J.M. Chabala, R. Levi-Setti, Dopant distributions in rare-earth-doped alumina, *J. Am. Ceram. Soc.* 80 (2) (1997) 373–376.
- [14] P. Gruffel, C. Carry, Effect of grain size on yttrium grain boundary segregation in fine-grained alumina, *J. European Ceram. Soc.* 11 (3) (1993) 189–199.
- [15] M.A. Gülgün, R. Voytovych, I. MacLaren, M. Rühle, R.M. Cannon, Cation segregation in an oxide ceramic with low solubility: yttrium doped  $\alpha$ -Alumina, *Interface Sci.* 10 (1) (2002) 99–110.
- [16] R.F. Cook, A.G. Schrott, Calcium segregation to grain boundaries in alumina, *J. Am. Ceram. Soc.* 71 (1) (1988) 50–58.
- [17] R. Akiva, A. Katsman, W.D. Kaplan, Anisotropic grain boundary mobility in undoped and doped alumina, *J. Am. Ceram. Soc.* 97 (5) (2014) 1610–1618.
- [18] R. Voytovych, I. MacLaren, M.A. Gülgün, R.M. Cannon, M. Rühle, The effect of yttrium on densification and grain growth in  $\alpha$ -alumina, *Acta Mater.* 50 (13) (2002) 3453–3463.
- [19] C.M. Wang, G.S. Cargill III, H.M. Chan, M.P. Harmer, Structural features of Y-saturated and supersaturated grain boundaries in alumina, *Acta Mater.* 48 (10) (2000) 2579–2591.
- [20] S.I. Bae, S. Baik, Determination of critical concentrations of silica and/or calcia for abnormal grain growth in alumina, *J. Am. Ceram. Soc.* 76 (4) (1993) 1065–1067.
- [21] M. Baram, W.D. Kaplan, Quantitative HRTEM analysis of FIB prepared specimens, *J. Microsc.* 232 (3) (2008) 395–405.
- [22] H. Müllejans, J. Bruley, Improvements in detection sensitivity by spatial difference electron energy-loss spectroscopy at interfaces in ceramics, *Ultramicroscopy* 53 (4) (1994) 351–360.
- [23] X.F. Zhang, Q. Yang, L.C. De Jonghe, Z. Zhang, Energy dispersive spectroscopy analysis of aluminium segregation in silicon carbide grain boundaries, *J. Microsc.-Oxf.* 207 (2002) 58–68.
- [24] David B. Williams, C. Barry Carter, *Transmission Electron Microscopy*, Springer, New York, 2009, pp. 639–662.
- [25] R. Akiva, A. Katsman, W.D. Kaplan, Anisotropic grain boundary mobility in undoped and doped alumina, *J. Am. Ceram. Soc.* 97 (5) (2014) 1610–1618.
- [26] V.J. Keast, D.B. Williams, Quantification of boundary segregation in the analytical electron microscope, *J. Microsc.* 199 (1) (2000) 45–55.
- [27] H. Meltzman, Y. Kauffmann, P. Thangadurai, M. Drozdov, M. Baram, D. Brandon, W.D. Kaplan, An experimental method for calibration of the plasmon mean free path, *J. Microsc.-Oxf.* 236 (3) (2009) 165–173.
- [28] K.F.J. Heinrich, T.D. McKinley, K.F.J. Heinrich, D. B. Wittry (Eds.), *The Electron Microprobe*, J. Wiley, New York, 1996, pp. 296–377.
- [29] U. Alber, H. Müllejans, M. Rühle, Improved quantification of grain boundary segregation by EDS in a dedicated STEM, *Ultramicroscopy* 69 (2) (1997) 105–116.
- [30] M.N. Kelly, S.A. Bojarski, G.S. Rohrer, The temperature dependence of the relative grain-boundary energy of yttria-doped alumina, *J. Am. Ceram. Soc.* 100 (2) (2017) 783–791.
- [31] G.S. Rohrer, The role of grain boundary energy in grain boundary complexion transitions, *Curr. Opin. Solid State Mater. Sci.* 20 (5) (2016) 231–239.
- [32] T. Gemming, S. Nufer, W. Kurtz, M. Rühle, Structure and chemistry of symmetrical tilt grain boundaries in  $\alpha$ -Al<sub>2</sub>O<sub>3</sub>: II, bicrystals with Y at the interface, *J. Am. Ceram. Soc.* 86 (4) (2003) 590–594.
- [33] M.A. Gülgün, V. Putlayev, M. Rühle, Effects of yttrium doping  $\alpha$ -Alumina: I, microstructure and microchemistry, *J. Am. Ceram. Soc.* 82 (7) (1999) 1849–1856.
- [34] D. Bouchet, F. Dupau, S. Lartigue-Korinek, Structure and chemistry of grain boundaries in yttria doped aluminas, *Microsc. Microanal. Microstruct.* 4 (6) (1993) 561–573.